

Supporting information

Nonpolar Solvent Effect by CH/ π Interaction inside Zeolites: Characterization, Mechanism and Concept

Guangchao Li^{[a][d][†]}, Ling Huang^{[a][†]}, Xianfeng Yi^[a], Yung-Kang Peng^[b], Shik Chi Edman Tsang^{[c]*}, Anmin Zheng^{[a]*}

^[a] State Key Laboratory of Magnetic Resonance and Atomic and Molecular Physics, National Center for Magnetic Resonance in Wuhan, Key Laboratory of Magnetic Resonance in Biological Systems, Wuhan Institute of Physics and Mathematics, Chinese Academy of Sciences, Wuhan 430071, P. R. China.

^[b] Department of Chemistry, City University of Hong Kong, Kowloon, Hong Kong, P. R. China.

^[c] The Wolfson Catalysis Centre, Department of Chemistry, University of Oxford, Oxford OX1 3QR, UK.

^[d] University of Chinese Academy of Sciences, Beijing 100049, P. R. China.

^[†] The authors contribute to this work equally.

*Corresponding authors: zhenganm@wipm.ac.cn; edman.tsang@chem.ox.ac.uk

List of Contents

Fig. S1. ^{13}C CP MAS NMR spectrum of ^{13}C -labeled acetone before (a) and after (b) co-adsorption with naphthalene on H-ZSM-5 zeolite at 298 K.

Fig. S2. XRD patterns of (a) H-MOR and (b) H-ZSM-5. The XRD measurements were conducted using $\text{CuK}\alpha$ radiation with a step size of 0.02° in a 2θ range of $5\text{--}70^\circ$ at a respective voltage of 40 kV and a current of 40 mA.

Fig. S3. ^1H , ^{27}Al , and ^{29}Si MAS NMR spectrum of H-ZSM-5 zeolites at 298 K in (a), (b) and (c), respectively. The dotted curves indicate results of spectral analyses by Gaussian deconvolution. The tetrahedral framework Al is represented by the peak at 54 ppm (b). For ^{29}Si spectra in (c), the peak at -106 ppm is assigned to $[\text{Si}(\text{OSi})_3\text{OAl}]$ and $[\text{Si}(\text{OSi})_3\text{OH}]$, while -112 and -115 ppm are devoted to $[\text{Si}(\text{OSi})_4]$.

Fig. S4. ^1H , ^{27}Al , and ^{29}Si MAS NMR spectrum of H-MOR zeolites at 298 K in (a), (b) and (c), respectively. The tetrahedral framework Al is represented by the peak at 54 ppm with octahedral species appearing -1 ppm (b). -107 and -117 ppm for ^{29}Si chemical shifts (c) are assigned to $[\text{Si}(\text{OSi})_3\text{OAl}]$ and $[\text{Si}(\text{OSi})_4]$, respectively.

Fig. S5. Optimized geometries of acetone (a) and co-adsorbed with naphthalene (b), benzene (c) inside the periodic unit cell of H-ZSM-5 zeolite. The selected interatomic (\AA) distances are indicated.

Fig. S6. Optimized structures for the two distinctive stable co-adsorption configurations of acetone and naphthalene in the ZSM-5 channel with their electronic energies relative to the reference state of b.

Fig. S7. ^{13}C CP MAS NMR spectrum of ^{13}C -labeled acetone before (b) and after (a) co-absorption with benzene on H-ZSM-5 zeolite. All the MAS NMR measurements were carried out by Bruker Avance III 400 WB spectrometer under 10 kHz at 298K.

Fig. S8. ^{13}C CP MAS NMR spectrum of ^{13}C -labeled acetone before (b) and after (a) co-absorption with benzene on H-MOR zeolite. All the MAS NMR measurements were carried out by Bruker Avance III 400 WB spectrometer under 10 kHz at 298K.

Fig. S9. Two-dimensional solid-state ^{13}C - ^1H hetero-nuclear correlation MAS NMR spectrum of ^{13}C labeled acetone and benzene co-adsorbed over H-ZSM-5 (a) and H-MOR (b) zeolites. All the MAS NMR measurements were carried out by Bruker Avance III 400 WB spectrometer under 10 kHz at 298 K.

Fig. S10. The device of vacuum system for adsorption.

Table S1. The calculated ^{13}C chemical shifts (δ_{iso}) of acetone (ace) in zeolite H-ZSM-5 surrounded with naphthalene (naph) and benzene (benz), the interatomic distance between carbonyl and the proton of Brønsted acid sites (Å).

Methods

Sample preparation and solid-state NMR experiment.

^{13}C -labeled acetone (ca. 98%, CLM-245-1) and powdered, binderless NH_4 -ZSM-5 ($\text{SiO}_2/\text{Al}_2\text{O}_3=50$, CBV 5524G) and NH_4 -MOR ($\text{SiO}_2/\text{Al}_2\text{O}_3=20$, CBV 21A) zeolites were purchased from Cambridge Isotope Laboratories, Inc. and Zeolyst International, respectively. Deamination of the commercial zeolites was conducted by dried at 383 K for 2 h, then calcined at 773 K for 6 h under flowing dry air. Subsequently the samples were performed on a vacuum line for dehydration. The temperature was gradually increased at a rate of 1 K/min and the samples were kept at a final temperature of 673 K at a pressure below 10^{-3} Pa over a period of 10 h. After the samples being cooled to ambient temperature, the dehydrated zeolites mixed with a certain amount of naphthalene (bought from Sigma-Aldrich, CAS: 91-20-3) in a glass tube, next the tube was heated in an oven at 433 K for 10 h, in order to let the naphthalene (m.p. 353 K) diffuse into the powder. And then evacuation at 298 K for 30 min on a vacuum line to eliminate physisorbed molecules. Subsequently, by reading the changes in the gas manometer (Figure S10), a known amount of 2- ^{13}C -acetone was introduced into the activated samples. Finally, the sample tubes were flame sealed. Prior to NMR experiments, the sealed sample was transferred into a ZrO_2 rotor with a Kel-F endcap under a dry nitrogen atmosphere in a glovebox. It is worth mentioning that before the adsorption, the quantities of naphthalene and 2- ^{13}C -acetone were confirmed according to the acid amounts in the two zeolites, making sure no more than one ^{13}C -2-acetone and one naphthalene per acid site (see Figure S10).

^1H , ^{13}C MAS NMR measurements were carried out using a Bruker Avance III 400 WB spectrometer at resonance frequencies of 399.33 and 104.22 MHz, respectively, ^1H MAS NMR spectra were acquired on a 4 mm probe with a spinning rate of 10 kHz, a $\pi/2$ pulse length of 3.8 μs , and a recycle delay of 5 s. While the samples used for the ^1H and MAS NMR studies were additionally dehydrated in vacuum at 673 K for 10 h before the measurements or the loading with the adsorption molecules. The ^{13}C CP and 2D ^1H - ^{13}C hetero-nuclear MAS NMR experiments were performed on a 4 mm probe with a contact time of 4 ms, a recycle delay of 2.5 s, and a sample spinning rate of 10 kHz. ^{27}Al , ^{29}Si MAS NMR experiments were carried out on a Varian InfinityPlus-300 spectrometer with the Larmor frequencies of 78.16, 59.59 MHz, respectively. ^{27}Al MAS NMR spectra were recorded with a pulse length of 0.2 μs ($<\pi/12$), a recycle delay of 1 s, and a spinning rate of 10 kHz. ^{29}Si MAS NMR spectra with high-power proton decoupling were recorded on a 7.5 mm probe with a spinning rate of 3.5 kHz, a $\pi/2$ pulse length of 5.2 μs , and a recycle delay of 80 s. Unlike the ^1H and ^{13}C NMR spectra, which were obtained from dehydrated samples, the ^{27}Al and ^{29}Si MAS NMR investigations were carried out with samples that were fully hydrated at ambient temperature overnight in a desiccator. The chemical shifts of ^1H , ^{13}C , ^{27}Al , ^{29}Si were referenced to adamantane, hexamethylbenzene, $\text{Al}(\text{NO}_3)_3$ (1 mol/L), and Kaolin, respectively.

Theoretical model for H-ZSM-5 & calculation methods

An initial single unit cell of ZSM-5 zeolite (1x1x1, $\text{Si}_96\text{O}_{192}$) retrieved from the IZA zeolites database was used in this work (Figure S5).¹ On the basis of the

accessibility of adsorbed molecules toward ZSM-5 zeolite, the T12–O24–T12 site in the intersection channel of the zeolite was chosen as the active site. for H-ZSM-5.² During the optimization, all the atoms of zeolite framework and adsorbed organic molecules were allowed to relax. the structural optimization presented in this work were performed using VASP software.^{3, 4} The generalized gradient approximation (GGA) under the scheme proposed by Perdew, Burke and Ernzerhof (PBE) was used,⁵ Grimme's method was added to the GGA energy to account for the long range-interactions (DFT-D3).⁶ The projector augmented wave (PAW) was used to describe electron-ion interaction with the plane wave basis set kinetic energy cutoff equal to 500 eV.^{7, 8} The sampling of Brillouinzone was only with Gamma point (1x1x1). The convergence criterion for the electronic self-consistency measured by the change in the total energy between successive iterations was set to 10^{-5} eV/u.c. Part of atomic positions was relaxed within a conjugate-gradient algorithm until all the forces acting on the atoms were lower than 0.03 eV/Å. The CASTEP NMR program with ab initio plane-wave DFT was performed to calculate ¹³C nuclear magnetic shielding and electric field gradient tensors employing the gauge including projector augmented wave (GIPAW) algorithm.⁹ Perdew, Burke, and Ernzerhof (PBE) functionals were adopted with the generalized gradient approximation (GGA) for the exchange correlation energy “on-the-fly” ultrasoft pseudopotentials provided in CASTEP was employed for calculation. Monkhorst-Pack k-point grid size of 1×1×1 and the cutoff energy of 500 eV was used for the convergence of the calculated NMR parameters. The calculations of noncovalent interaction reduced density gradient, the differential charge density as

well as molecular electrostatic potential were performed based on the Multiwfn program.¹⁰

All the images related to the theoretical calculation were obtained with the code Visualization for Electronic and Structural Analysis (VESTA 3.4)¹¹ and Visual molecular Dynamics (VMD 1.9.3)¹²

Noncovalent interaction reduced density gradient (RDG)

The noncovalent interaction index approach, which was developed by Yang et al.,¹³ was utilized in this work to visualize the nonbonding interactions between the co-adsorption molecules. The reduced density gradient (RDG), defined as $s = (1/(2(3\pi^2)^{1/3}))(|\Delta\rho(r)|/(\rho(r)^{4/3}))$, together with the electron density ρ , was used to distinguish the covalent and noncovalent interactions. In principle, the noncovalent interactions locate in the regions with low density and low RDG. The sign of the second largest eigenvalue (λ_2) of the electron density Hessian can be used to distinguish bonded ($\lambda_2 < 0$) from nonbonded ($\lambda_2 > 0$) interactions. Generally, the analysis of the sign of λ_2 can help to discern different types of noncovalent interactions: ($\text{sign}(\lambda_2)\rho < 0$, H-bonding interactions; $\text{sign}(\lambda_2)\rho \approx 0$, weak van der Waals interactions and $\text{sign}(\lambda_2)\rho > 0$, strong repulsive interaction). All the functions RDG and $\text{sign}(\lambda_2)\rho$ were calculated with the Multiwfn software.¹⁰

Differential charge density

The charge density difference for the configurations is calculated according to the equation:^{14, 15}

$$\Delta\rho = \rho_{AN} - \rho_A - \rho_N \quad (1)$$

where the ρ_{AN} term corresponds to the electronic density of the whole system including the co-adsorption states of acetone (A) and naphthalene (N), while the charge density of acetone molecule is represented by the ρ_A term. The electronic density of the isolated naphthalene molecule is denoted by the ρ_N term. We have used the same grid of points to represent the charge density and the same box size for all the calculations.

Molecular electrostatic potential (MEP)

Molecular electrostatic potential (MEP) is a powerful predictive and interpretive tool to rationalize trends in molecular reactivity, binding in host/guest complexes and intermolecular noncovalent interactions.^{16, 17} The MEP value $V(r)$ at position r in the molecular space is defined and calculated according to the equation:

$$V_{QM}(r) = \left\langle \Psi \left| \frac{1}{r} \right| \Psi \right\rangle = \sum_{A=1}^n \frac{Z_A}{|R_A - r|} - \sum_{\mu, \nu} P_{\mu\nu} \int \frac{\phi_{\mu}^*(r') \phi_{\nu}(r')}{|r' - r|} v dr'$$

where Ψ is the wave function of molecule A, Z_A and R_A are the charge and position of nucleus A, respectively, n is the number of component atoms, $P_{\mu\nu}$ are elements of density matrix, and μ and ν are indices of basic functions ϕ_{μ} and ϕ_{ν} , all in atomic units. The integral in the above equation runs over all molecular space. The electrostatic interaction energy between molecule A and a point charge q_k can be easily evaluated as follows:

$$E_A(r_{A,k}) = V_A(r_{A,k})q_k$$

where $V_A(r_{A,k})$ is the MEP of molecule A at distance $r_{A,k}$ between molecule A and

charge q_k .

Characterization of parent H-ZSM-5 and H-MOR zeolites.

Firstly, the structure and crystalline nature of the selected zeolites were examined by means of powder X-ray diffraction (XRD) patterns (Figure S2). The advanced solid-state NMR spectroscopies of ^1H , ^{27}Al , ^{29}Si on the parent H-ZSM-5 and H-MOR zeolites were performed as well. For H-ZSM-5 zeolite, the pristine catalyst contains three framework tetrahedral $\text{Si}(\text{Q}_4)$ features (Figure S3c): two peaks at -112.0 and -115.0 ppm are assigned to tetrahedral Si with four Si neighbors (i.e., $\text{Si}(\text{OSi})_4$),¹⁸ and one peak at -106 ppm is assigned to tetrahedral Si with either three Si and one Al (i.e., $\text{Si}(\text{OSi})_3(\text{OAl})$) or three Si and one hydroxy (i.e. $\text{Si}(\text{OSi})_3\text{OH}$), since the ^1H chemical resonances at 4.2 and 1.7 ppm (Figure S3a) can be assigned to the proton of Brønsted acid site and the silicon hydroxyl, respectively.^{19,20} Besides, only a single sharp signal at 54 ppm for the ^{27}Al chemical shifts is observed without any obvious signal of extra framework aluminum (EFAL) signal (Figure S3b).¹⁸ Similar results were also observed for the parent H-MOR zeolite, except that there is a small number of six-coordination extra framework aluminum (EFAL) species derived from the presence of weak -1.0 ppm peak in the chemical shift of ^{27}Al as shown Figure S4, suggesting the parent H-MOR zeolite has partly dealuminated.

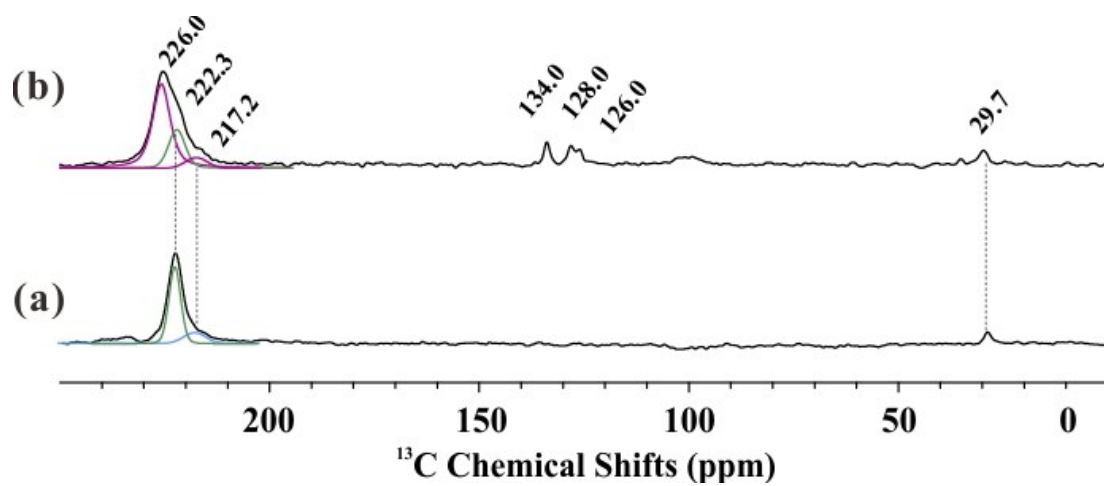


Figure S1 ^{13}C CP MAS NMR spectrum of ^{13}C -labeled acetone before (a) and after (b) co-adsorption with naphthalene on H-ZSM-5 zeolite at 298 K.

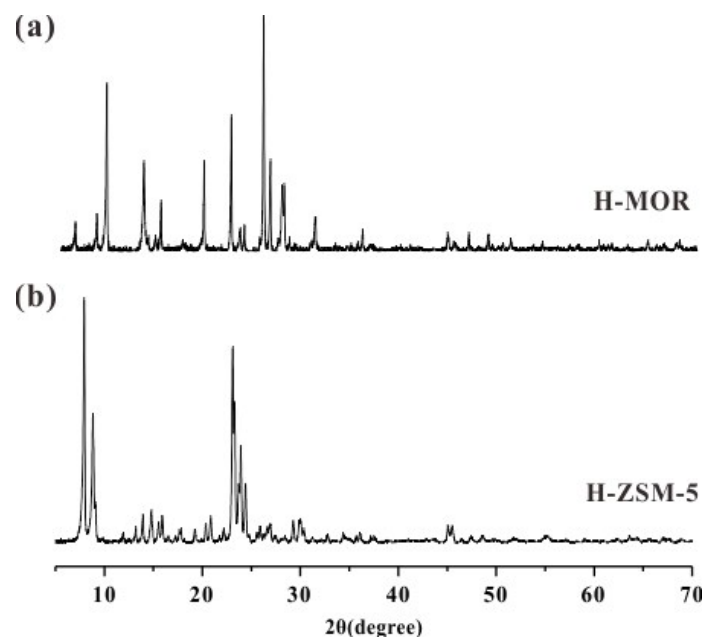


Figure S2. XRD patterns of (a) H-MOR and (b) H-ZSM-5. The XRD measurements were conducted using $\text{CuK}\alpha$ radiation with a step size of 0.02° in a 2θ range of $5\text{--}70^\circ$ at a respective voltage of 40 kV and a current of 40 mA.

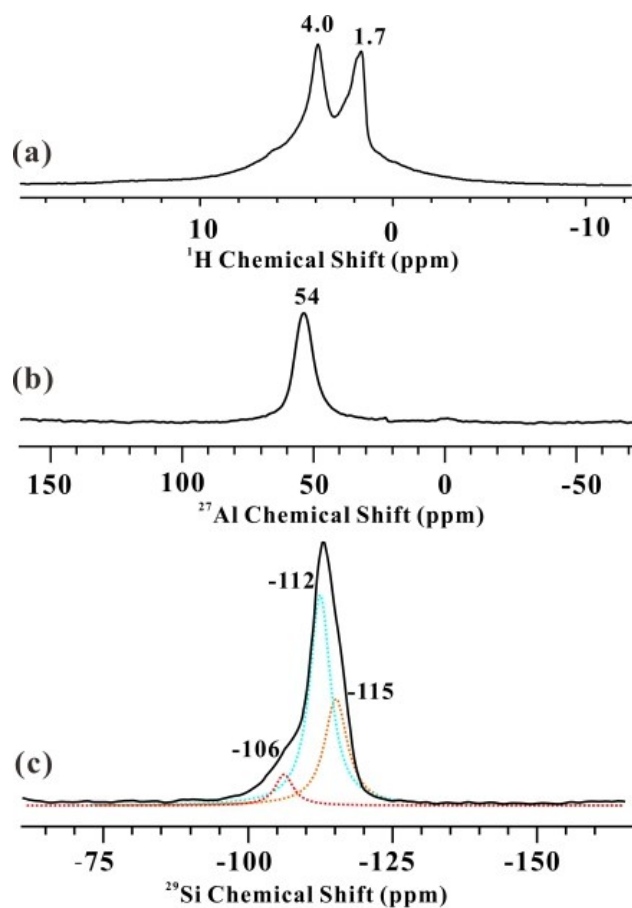


Figure S3. ^1H , ^{27}Al , and ^{29}Si MAS NMR spectrum of H-ZSM-5 zeolites at 298 K in (a), (b) and (c), respectively. The dotted curves indicate results of spectral analyses by Gaussian deconvolution. The tetrahedral framework Al is represented by the peak at 54 ppm (b). For ^{29}Si spectra in (c), the peak at -106 ppm is assigned to $[\text{Si}(\text{OSi})_3\text{OAl}]$ and $[\text{Si}(\text{OSi})_3\text{OH}]$, while -112 and -115 ppm are devoted to $[\text{Si}(\text{OSi})_4]$.

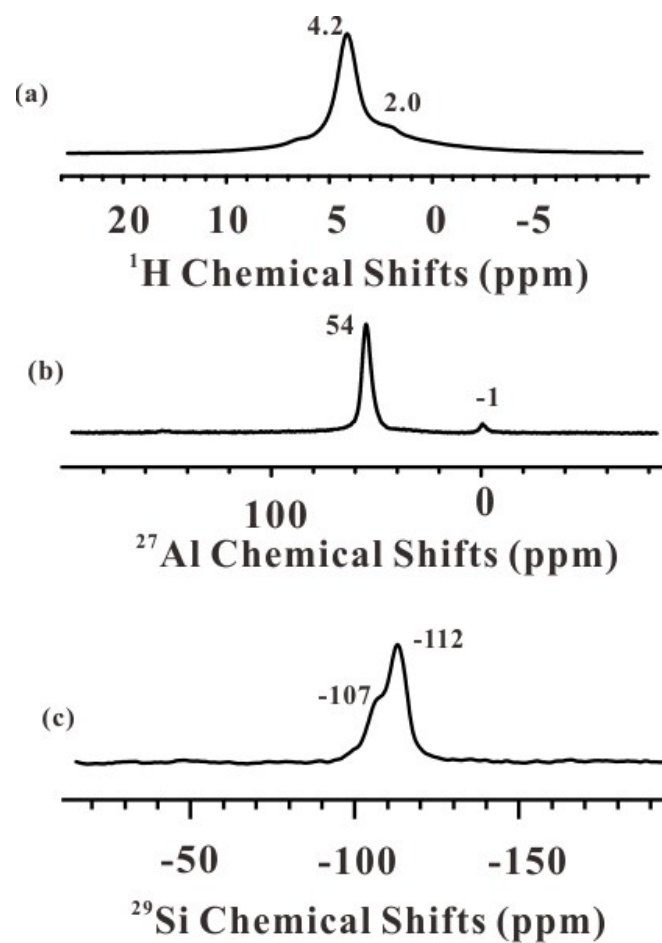


Figure S4. ^1H , ^{27}Al , and ^{29}Si MAS NMR spectrum of H-MOR zeolites at 298 K in (a), (b) and (c), respectively. The tetrahedral framework Al is represented by the peak at 54 ppm with octahedral species appearing -1 ppm (b). -107 and -117 ppm for ^{29}Si chemical shifts (c) are assigned to $[\text{Si}(\text{OSi})_3\text{OAl}]$ and $[\text{Si}(\text{OSi})_4]$, respectively.

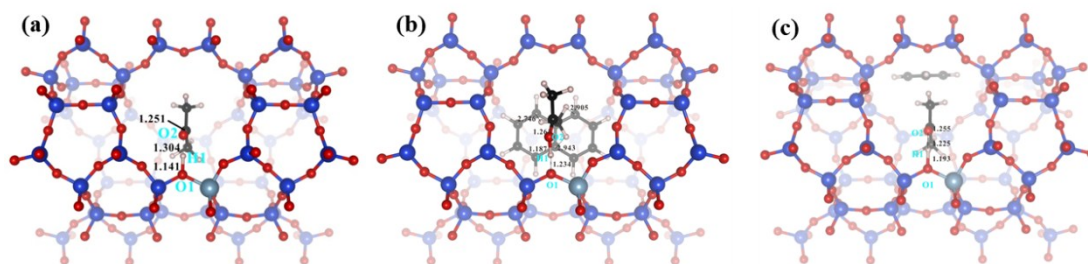


Figure S5. Optimized geometries of acetone(a) and co-adsorbed with naphthalene(b), benzene(c) inside the periodic unit cell of H-ZSM-5 zeolite. The selected interatomic (\AA) distances are indicated.

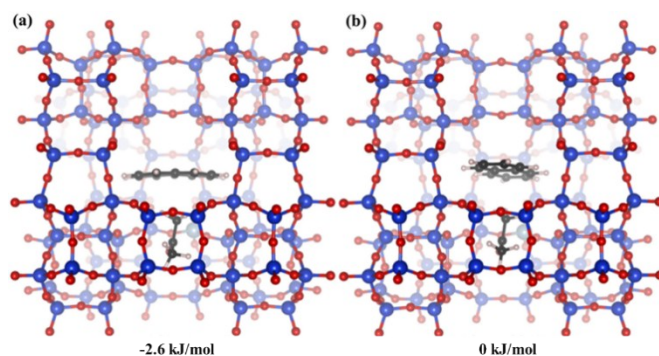


Figure S6. Optimized structures for the two distinctive stable co-adsorption configurations of acetone and naphthalene in the ZSM-5 channel with their electronic energies relative to the reference state of b.

The framework type MFI of ZSM-5 zeolite, which is built by using units of 12 SiO₄ tetrahedra (T) positioned at 12 distinct T sites, is characterized by a three-dimensional pore system with straight channels ($5.3 \times 5.6 \text{ \AA}^2$) in the [010] direction intersected by the zigzag channels ($5.1 \times 5.5 \text{ \AA}^2$) in the [100] direction. As mentioned in the main text, the T12-O24-T12 sites in the intersection channel of the zeolite were chosen as the active sites, which were easily accessible to the reactant molecules and they were considered among the most stable sites for Al substitution. For the co-adsorption structures, different configurations are considered as depicted in (Figure S6). Based the electronic energy, the most stable structure is selected, namely structure a that naphthalene is parallel to the axis of straight channel.

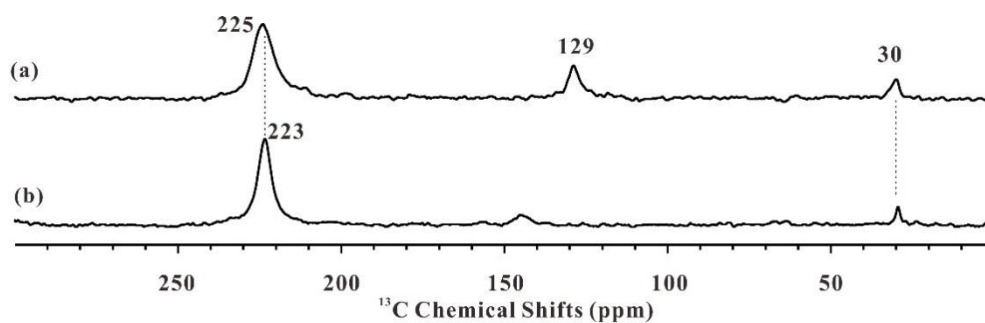


Figure S7. ^{13}C CP MAS NMR spectrum of ^{13}C -labeled acetone before (b) and after (a) co-absorption with benzene on H-ZSM-5 zeolite. All the MAS NMR measurements were carried out by Bruker Avance III 400 WB spectrometer under 10 kHz at 298K.

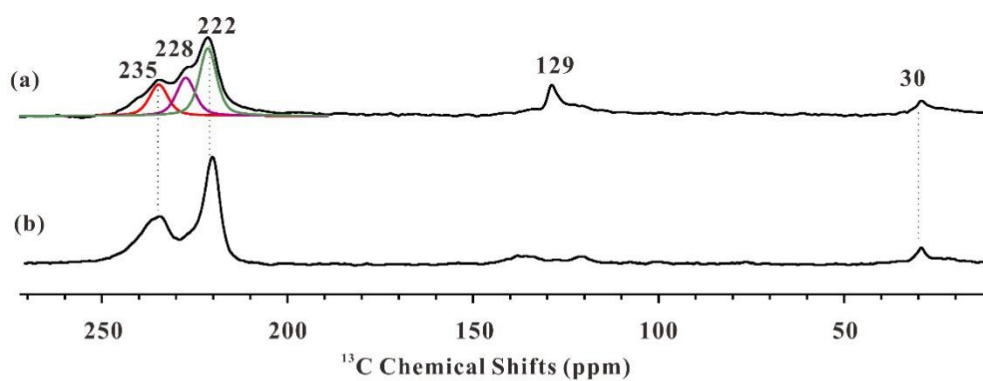


Figure S8. ^{13}C CP MAS NMR spectrum of ^{13}C -labeled acetone before (b) and after (a) co-absorption with benzene on H-MOR zeolite. All the MAS NMR measurements were carried out by Bruker Avance III 400 WB spectrometer under 10 kHz at 298K.

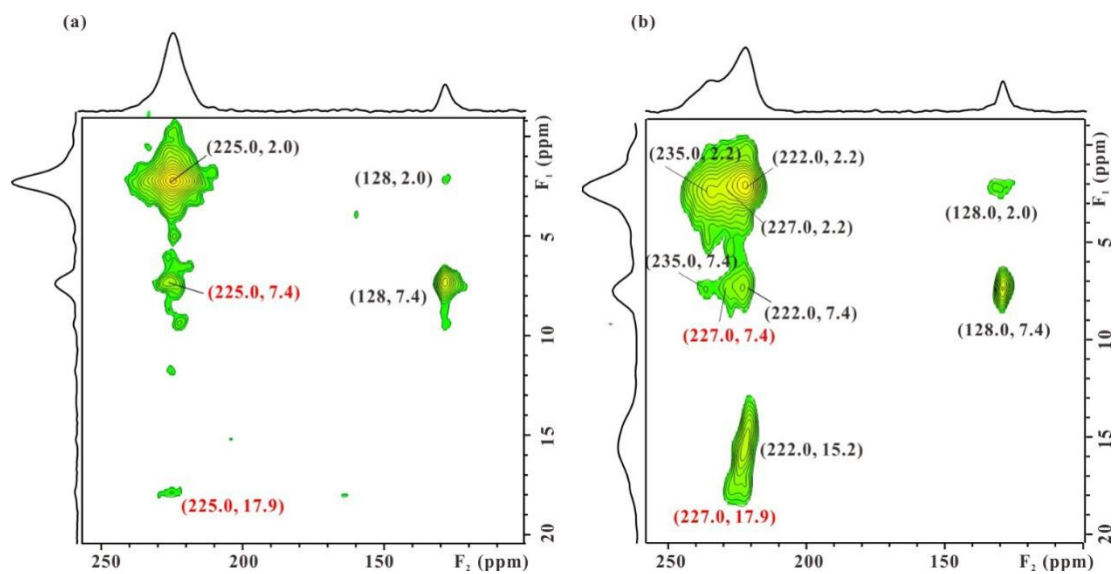


Figure S9. Two-dimensional solid-state ^1H - ^{13}C hetero-nuclear correlation MAS NMR spectrum of ^{13}C labeled acetone and benzene co-adsorbed over H-ZSM-5 (a) and H-MOR (b) zeolites. All the MAS NMR measurements were carried out by Bruker Avance III 400 WB spectrometer under 10 kHz at 298K.

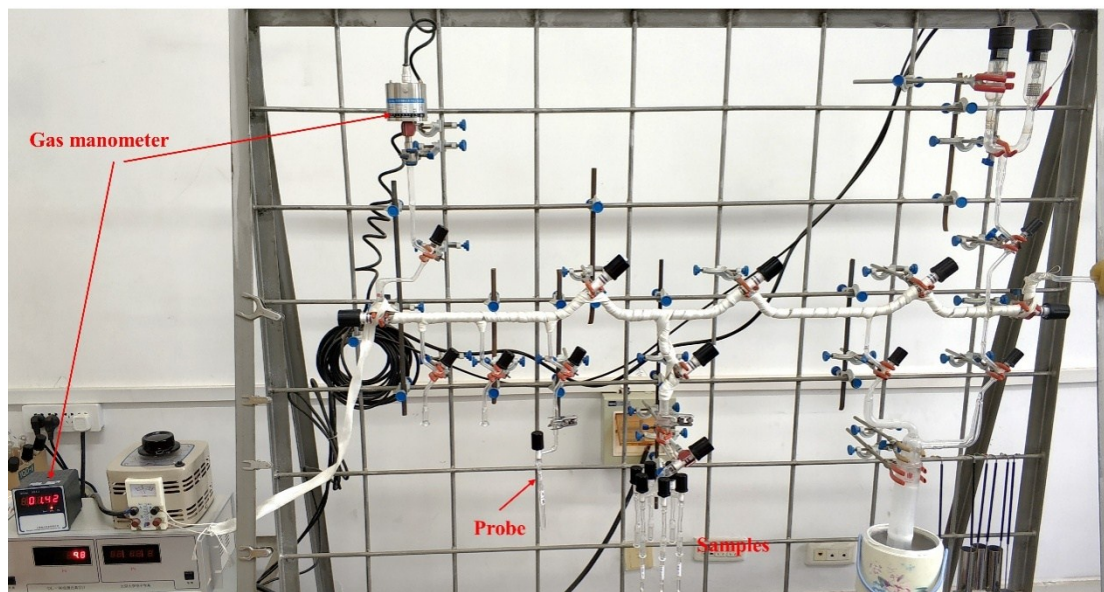


Figure S10. The device of vacuum system for adsorption.

a) Number of active sites per unit cell

- 1) In unit cell : $N(\text{Si})+N(\text{Al})= N(\text{T})$, $N(\text{Si}) \div N(\text{Al})= \text{ratio of Si/Al}$,
 $T(\text{H-MOR})=48$, $T(\text{H-ZSM-5})=96$
- 2) For H-MOR, $\text{Si/Al}=10$.
 $N(\text{Al})= 4.8$
- 3) For H-ZSM-5, $\text{Si/Al}=25$.
 $N(\text{Al})= 3.7$

There are average 4.8, 3.7 acid sites in each unit cell for our selected H-MOR and H-ZSM-5, respectively.

b) Total number of active sites

- 1) The Si/Al of H-MOR and H-ZSM-5 are 10 and 25, respectively.
- 2) For 1 g zeolites
 $n(\text{zeolite unit cell}) = 1 \text{ g} \div M(\text{zeolite unit cell})$
- 3) For H-MOR
 $n(\text{H-MOR unit cell}) = 1 \text{ g} \div M(\text{Si}_48\text{O}_96) = 1 \text{ g} \div 2884 \text{ g} \cdot \text{mol}^{-1} = 3.5 \times 10^{-4} \text{ mol}$
 $n(\text{acid sites}) = N(\text{Al}) \times n(\text{H-MOR unit cell}) = 4.8 \times 3.5 \times 10^{-4} \text{ mol} = 1.68 \text{ mmol}$
- 4) For H-ZSM-5
 $n(\text{H-ZSM-5 unit cell}) = 1 \text{ g} \div M(\text{Si}_96\text{O}_{192}) = 1 \text{ g} \div 5768 \text{ g} \cdot \text{mol}^{-1} = 1.7 \times 10^{-4} \text{ mol}$
 $n(\text{acid sites}) = N(\text{Al}) \times n(\text{H-ZSM-5 unit cell}) = 3.7 \times 1.7 \times 10^{-4} \text{ mol} = 0.629 \text{ mmol}$

Table S1. The calculated ^{13}C shielding and chemical shifts of acetone in zeolite H-ZSM-5 surrounded with naphthalene and benzene, the interatomic distance between carbonyl and the proton of Brønsted acid sites.

absorbate	NMR parameter (ppm)		Bond length (Å)		
	^{13}C shielding	^{13}C chemical shift	C=O2	O2-H1	H1-O1
acetone	-69.4	223.0	1.251	1.304	1.141
acetone/naphthalene	-73.6	227.2	1.261	1.187	1.234
acetone/benzene	-71.3	224.9	1.255	1.225	1.193

References

1. C. Baerlocher, McCusker, L.B. <http://www.iza-online.org/>
2. K. P. Schroder, J. Sauer, M. Leslie and C. R. A. Catlow, *Zeolites*, 1992, **12**, 20-23.
3. G. Kresse and J. Furthmuller, *Comput. Mater. Sci.*, 1996, **6**, 15-50.
4. G. Kresse and J. Furthmuller, *Phys. Rev. B*, 1996, **54**, 11169-11186.
5. J. P. Perdew, K. Burke and M. Ernzerhof, *Phys. Rev. Lett.*, 1996, **77**, 3865-3868.
6. S. Grimme, J. Antony, S. Ehrlich and H. Krieg, *J. Chem. Phys.*, 2010, **132**.
7. P. E. Blochl, *Phys. Rev. B*, 1994, **50**, 17953-17979.
8. G. Kresse and D. Joubert, *Phys. Rev. B*, 1999, **59**, 1758-1775.
9. S. J. Clark, M. D. Segall, C. J. Pickard, P. J. Hasnip, M. J. Probert, K. Refson and M. C. Payne, *Z. Kristallogr.*, 2005, **220**, 567-570.
10. T. Lu and F. Chen, *J. Comput. Chem.*, 2012, **33**, 580-592.
11. K. Momma and F. Izumi, *J. Appl. Crystallogr.*, 2011, **44**, 1272-1276.
12. W. Humphrey, A. Dalke and K. Schulten, *J. Mol. Graph. Model.*, 1996, **14**, 33-38.
13. E. R. Johnson, S. Keinan, P. Mori-Sanchez, J. Contreras-Garcia, A. J. Cohen and W. Yang, *J. Am. Chem. Soc.*, 2010, **132**, 6498-6506.
14. Y. Chu, B. Han, A. Zheng, X. Yi and F. Deng, *J. Phys. Chem. C*, 2013, **117**, 2194-2202.
15. Y. Chu, B. Han, A. Zheng and F. Deng, *J. Phys. Chem. C*, 2012, **116**, 12687-12695.
16. J. S. Murray and P. Politzer, *WIREs. Comput. Mol. Sci.*, 2011, **1**, 153-163.
17. Q.-S. Du, C.-H. Wang, Y.-T. Wang and R.-B. Huang, *J. Phys. Chem. B*, 2010, **114**, 4351-4357.
18. Z. Yu, S. Li, Q. Wang, A. Zheng, X. Jun, L. Chen and F. Deng, *J. Phys. Chem. C*, 2011, **115**, 22320-22327.
19. H. Koller and M. Weiß, in *Solid State NMR*, Springer, Berlin Heidelberg, 2011, pp. 189-227.
20. A. Zheng, S.-J. Huang, Q. Wang, H. Zhang, F. Deng and S.-B. Liu, *Chin. J. Catal.*, 2013, **34**, 436-491.